scientific reports

Check for updates

OPEN

Study on CO_2/CH_4 displacement process in shale microscale models with adsorption/desorption behavior by lattice Boltzmann method

Yifu Zhang[1], Yu Xu[2]✉, Xuefeng Chen[1], Zikun Pi[1], Qiannan Xie[1] & Kunpeng Liao[1]

The competitive adsorption of CH_4/CO_2 in shale has consistently garnered significant attention as a means to enhance the recovery efficiency of shale gas reservoirs. A theoretical formula for a binary gas competitive adsorption rate model was formulated to investigate the adsorption and desorption characteristics and the evolution patterns of carbon dioxide (CO_2) displacing methane (CH_4) in shale. This formula was integrated into the lattice Boltzmann method (LBM) to simulate the displacement process of CH_4 by CO_2, addressing competitive adsorption challenges associated with binary gases exhibiting adsorption/desorption behaviors. The research findings reveal that the proposed theoretical model accurately captures the competitive adsorption dynamics between CO_2 and CH_4, elucidating the patterns of adsorption and desorption characteristics during the displacement of CH_4 by CO_2. This insight is pivotal for understanding the microscopic mechanisms underlying CO_2-induced CH_4 displacement. The displacement process is dynamic, marked by concurrent adsorption and desorption of CO_2 and CH_4, ultimately converging to an equilibrium state where CO_2 adsorption and CH_4 desorption coexist. Notably, the time taken for CO_2 to attain equilibrium is marginally delayed compared to CH_4. Moreover, the concentration of injected CO_2 substantially influences the dynamics of CO_2 replacing CH_4, as the CO_2 injection concentration increases, both the adsorption rate of CO_2 and the desorption rate of CH_4 augment, while the time required to reach equilibrium in the adsorption/desorption process diminishes. This implies that CO_2 injection effectively facilitates CH_4 desorption. Additionally, models with higher porosity exhibit enhanced permeability, resulting in accelerated adsorbate diffusion rates and improved displacement efficiency. The heterogeneity of the pore structure exerts a pronounced impact on the velocity distribution within the flow field, which in turn significantly influences the concentration field distribution of CO_2 and CH_4. It is worth noting that the distribution characteristics of the two gases within the flow field and their concentrations within the particles are complementary. The results underscore that carbon dioxide injection can enhance methane desorption, thereby improving shale gas recovery.

Keywords Numerical simulation, Adsorption/desorption behavior, Porous media, Displacement process, Lattice Boltzmann method

Nanoscale pores in shale serve dual functions: as storage spaces for shale gas and effective sequestration sites for greenhouse gases[1,2]. The CO_2-Enhanced Shale Gas Recovery (CO_2-ESGR) technology is regarded as an auspicious approach, as it simultaneously facilitates shale gas development and CO_2 sequestration, positioning it as a current focal point of research[3]. Shale gas primarily exists in nanoscale storage spaces in two forms: adsorbed and free states. These states involve various migration mechanisms, including adsorption/desorption, diffusion, and viscous flow[4]. Particularly under primary reservoir conditions, the displacement and competitive adsorption behaviors of multicomponent gases occur within the porous media[5]. The mechanisms underlying

[1]School of Safety and Management Engineering, Hunan Institute of Technology, Hengyang 421002, China. [2]School of Resources and Safety Engineering, Central South University, Changsha 410083, China. ✉email: xy1235813@csu.edu.cn

these behaviors remain unclear and represent a significant scientific challenge in achieving CO_2-enhanced shale gas recovery.

Shale reservoir spaces, characterized by their highly complex internal structures, are macroscopically represented as a porous media system dominated by heterogeneous pores and fracture networks[6]. In such intricate porous media, the transport processes of multi-component gases exhibit significantly nonlinear dynamic behaviors, presenting substantial challenges in deciphering their core mechanisms at the laboratory scale[7]. From a physical mechanisms perspective, these phenomena fundamentally relate to fluid–solid coupling issues under complex boundary conditions, often accompanied by multi-physics coupling effects, including heat transfer, mass transfer, and multiphase flow[8]. The interaction of multiple physical fields directly results in solutions to their governing equations being constrained by both strong nonlinearity and high computational complexity. The lattice Boltzmann method (LBM) has been extensively utilized by the academic community for the numerical simulation of relevant physical processes, addressing this research challenge and providing a reliable technical approach for elucidating scientific mechanisms and exploring engineering solutions[9].

Ren et al.[10] combined the real gas state equation with the lattice Boltzmann method to investigate the microflow characteristics of shale gas within a simplified microchannel physical model by further discussing the boundary slip velocity and pressure distribution under different parameters. Luo et al.[11] utilized the lattice Boltzmann method to simulate double diffusion mixed convection, fluid–solid conjugate heat transfer, and the adsorption process at the pore scale within a lid-driven composite enclosure filled with a homogeneous medium by discussing the effects of the buoyancy ratio and adsorption rate on heat and mass transfer within the computational model. Yang et al.[12] used LBM to investigate the flow-coupled mass transfer process of CO_2 adsorption in flue gas by ZIF-8 material at REV scale, including the effects of porosity, arrangement, and particle size on CO_2 adsorption capacity.

However, these researches were conducted within artificially constructed, regularly shaped packing channels, without taking into account the randomness and complexity inherent in the internal structure of porous media. In order to express the porous characteristics of shale micropores, the Quart Structure Generation Set (QSGS) method[13] provides a feasible approach for the generation of random porous media. This method can generate porous media samples with different structures and properties by controlling four parameters: porosity, pore size distribution, pore shape distribution, and pore arrangement distribution. Zhou et al.[14] conducted numerical studies on the gas–solid adsorption process in reconstructed random porous media using the lattice Boltzmann method. Their work provides detailed insights into the effects of internal and external mass transfer resistance, offering theoretical guidance for the design and optimization of adsorption systems. Similarly, Wang et al.[15] developed a numerical model for the flow, heat transfer, and mass transfer of flashing vapor within porous media using LBM. Their study focused on the adsorption/desorption characteristics and thermal effects of LNG flashing vapor under cryogenic storage conditions.

The process of CO_2 displacing CH_4 within the pores of shale matrices serves as the primary mechanism underlying CO_2-Enhanced Shale Gas Recovery (CO_2-ESGR)[16] technology. Consequently, it is imperative to explore the competitive adsorption and miscible displacement processes between CO_2 and CH_4. Most researchers have concentrated on the adsorption characteristics of single-component gases, whereas relatively few studies have investigated the competition and displacement among multiple gas components[17]. Wu et al.[5] utilized the lattice Boltzmann method to simulate the CO_2/CH_4 displacement in a nanoporous shale matrix by integrating the Navier–Stokes equations with multicomponent advection–diffusion equations. Their findings indicated that the global mass transfer process is susceptible to intra-matrix diffusion; selectivity can significantly influence the outflux concentration when the solid diffusion rate is approximately 10^{-4} of the bulk diffusion rate. Nevertheless, there is still a lack of sufficient theoretical support for the competitive adsorption and displacement processes involving multi-component gases. Furthermore, our current understanding of the adsorption and desorption characteristics of gases during the CO_2 displacement of CH_4 remains limited and requires further investigation.

Unlike previous studies, this paper establishes a theoretical model for the competitive adsorption behavior of binary gases within porous media, providing sufficient theoretical support for research on the competitive adsorption and displacement characteristics of multi-component gases. Utilizing the LBM method, the adsorption/desorption characteristics during the CO_2/CH_4 displacement process at the microscale in shale are analyzed. The technical requirements for contemporary shale gas extraction and carbon sequestration are explored, offering robust assistance for the study of the mechanism of CO_2-enhanced shale gas recovery.

Two-component gas competitive adsorption model

The process of gas adsorption by solids involves convection, heat transfer, and mass transfer within the pore channels of a mixed fluid. Additionally, this process encompasses gas adsorption on the surface of particles, along with diffusion and heat transfer within the particles. Figure 1 illustrates the overall framework of the adsorption model.

The physical model of the simulation consists of a two-dimensional channel filled with a disordered random porous medium. For simplicity, circular adsorbent particles with complex internal pore structures represent the random porous medium. Given the low velocity in the porous model, the fluid adheres to the assumption of incompressible flow[18]. This study considers only adsorption, desorption, and diffusion, while neglecting changes in pore and matrix porosity, as well as alterations in the reaction front caused by dissolution reactions. The adsorption behavior of gases on solid surfaces is a dynamic process that involves simultaneous adsorption and desorption[19]. Figure 1 presents a detailed schematic diagram illustrating mass transport during adsorption. Gases such as carbon dioxide and methane are transferred to the surface of particulate matter through convection and diffusion. Initially, the adsorbate is adsorbed onto the outer surface of the particles via surface adsorption, and it subsequently diffuses into the micropores of the adsorbent through intraparticle diffusion. It is important to

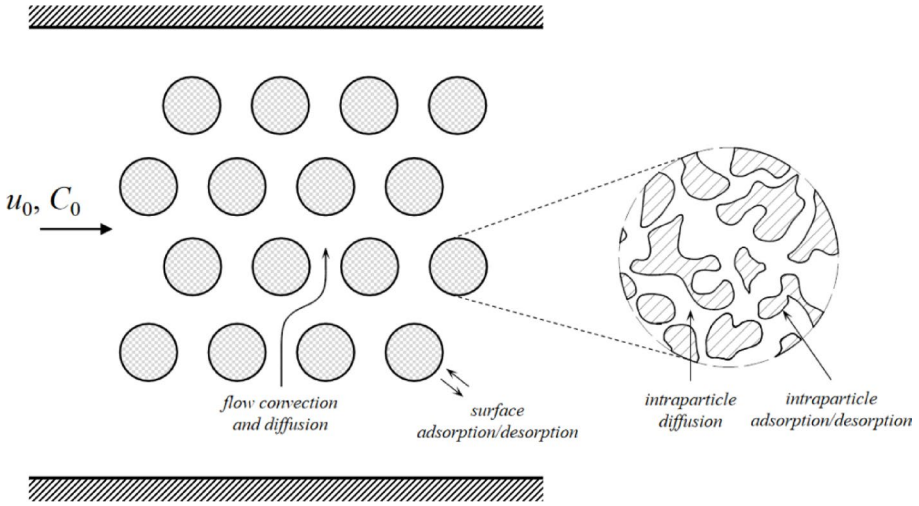

Fig. 1. Schematic of the adsorption/desorption process in a channel filled with adsorbent particles.

note that, due to the small size of the micropores, the convection effect within them is negligible; therefore, only the diffusion effect of the adsorbate is considered following this simplification.

Based on the assumption of single-layer physical adsorption and the Langmuir Eq. [20], when two adsorbates A and B compete for the same adsorption site, the expressions of the adsorption rate v_a and desorption rate are v_d:

$$v_{a,A} = k_{a,A} p_A \left(1 - \theta_A - \theta_B\right), v_{a,B} = k_{a,B} p_B \left(1 - \theta_A - \theta_B\right) \tag{1}$$

$$v_{d,A} = k_{d,A} \theta_A, v_{d,B} = k_{d,B} \theta_B \tag{2}$$

where p is the partial pressure of gas phase adsorbate, θ is the surface coverage, indicating the fraction of solid surface adsorption sites covered, k_a and k_d are the adsorption and desorption rate constants, respectively.

Combining formulas (1) and (2) and denoting the adsorption equilibrium constant b as:

$$b = \frac{k_a}{k_d} \tag{3}$$

the coverage of the two components on the adsorbent surface can be obtained as:

$$\theta_A = \frac{b_A p_A}{1 + b_A p_A + b_B p_B}, \theta_B = \frac{b_B p_B}{1 + b_A p_A + b_B p_B} \tag{4}$$

According to the definition of surface coverage, it can be expressed as:

$$\theta_A = \frac{V_A}{V_m}, \theta_B = \frac{V_B}{V_m} \tag{5}$$

where V_m is the Langmuir volume, which represents the maximum adsorbed volume at infinite pressure.

Substituting Eq. (5) into Eq. (4) and organizing it, the expression for the equilibrium adsorption volume of the adsorbate can be obtained:

$$V_A = \frac{V_m p_A}{\frac{1}{b_A} + \frac{b_B}{b_A} p_B + p_A}, V_B = \frac{V_m p_B}{\frac{1}{b_B} + \frac{b_A}{b_B} p_A + p_B} \tag{6}$$

Assuming ideal gas behavior, the pressure can be expressed as $p = \frac{1}{\gamma} C M c_s^2$ and denote b'_A and b'_B as follows:

$$b'_A = \frac{b_A}{\gamma} M c_s^2, b'_B = \frac{b_B}{\gamma} M c_s^2 \tag{7}$$

where M is molar mass (g/mol) , C is concentration of free gas (kmol/m^3), γ is the adiabatic index and c_s is sound speed (m/s).

The equilibrium adsorption volume of the adsorbate can be expressed as:

$$V_A = \frac{V_m C_A}{\frac{1}{b'_A} + \frac{b'_B}{b'_A} C_B + C_A}, V_B = \frac{V_m C_B}{\frac{1}{b'_B} + \frac{b'_A}{b'_B} C_A + C_B} \tag{8}$$

Considering the dynamic adsorption/desorption process and the competitive adsorption behavior of the two-component gas, the adsorption rate equations for adsorbates A and B under the monolayer assumption are given by:

$$\frac{\partial V_A}{\partial t} = k_{a,A} C_A \left(V_m - V_A\right) - k_{d,A} V_A \left(1 + \frac{k_{a,B}}{k_{d,B}} C_B\right) \tag{9-1}$$

$$\frac{\partial V_B}{\partial t} = k_{a,B} C_B \left(V_m - V_B\right) - k_{d,B} V_B \left(1 + \frac{k_{a,A}}{k_{d,A}} C_A\right) \tag{9-2}$$

When adsorption reaches equilibrium, the above two equations can be reduced to the form of the Langmuir adsorption kinetics Eqs. (8) for adsorbates A and B, when two-component gases compete for the same adsorption sites.

LBM model of two-component gas flow and competitive adsorption

LBM model describing gas flow

In this paper, the lattice Boltzmann method (LBM) is employed to simulate the flow of two-component gases in complex structures. The evolution equation for the density distribution function f of CO_2-CH_4 mixture is given by:

$$f_i\left(\mathbf{r} + e_i \Delta t, t + \Delta t\right) = f_i\left(\mathbf{r}, t\right) - \frac{1}{\tau_f}\left[f_i\left(\mathbf{r}, t\right) - f_i^{eq}\left(\mathbf{r}, t\right)\right] \tag{10}$$

where $f_i^{eq}(r,t)$ is the equilibrium distribution function at position $\boldsymbol{r}$ at time t, Δt is the time step, τ_f is the dimensionless relaxation (collision) time and e_i represents the lattice velocity in the i-th direction. $f_i^{eq}(r,t)$ is the equilibrium distribution function. The expressions are given as follows:

$$f_i^{eq}\left(\mathbf{r}, t\right) = w_i \rho \left[1 + \frac{e_i \cdot \mathbf{u}}{c_s^2} + \frac{\left(e_i \cdot \mathbf{u}\right)^2}{2c_s^4} - \frac{\mathbf{u} \cdot \mathbf{u}}{2c_s^2}\right] \tag{11}$$

where $\boldsymbol{u}$ is the macroscopic velocity.

Figure 1 depicts a physical model with a relatively large Knudsen number. When Kn > 10, due to the free molecular flow state of shale gas, the pore walls of shale are rough and there is adsorption behavior. Using non-slip boundary conditions is more in line with the real situation. In addition, in free molecular flow, intermolecular collisions can be ignored, and the physical meaning of traditional viscosity disappears. The definition and role of viscosity coefficient need to be re examined. Therefore, the relaxation time needs to be revised through effective viscosity[21]

$$\tau_f = \frac{1}{2} + \frac{\nu_f}{\Delta t c_s^2} \frac{1}{1 + \frac{4}{\pi} Kn \arctan\left(\sqrt{2} Kn^{-3/4}\right)} \tag{12}$$

where v_f represents the kinematic viscosity of the fluid; Kn is the Knudsen number; c_s is the lattice sound speed.

In the physical modeling of gas flow, the D2Q9 lattice model[22], which employs a two-dimensional nine-velocity scheme, is utilized to discretize particle velocities within a two-dimensional space.

$$e_i = c \begin{pmatrix} 0 & 1 & 0 & -1 & 0 & 1 & -1 & -1 & 1 \\ 0 & 0 & 1 & 0 & -1 & 1 & 1 & -1 & -1 \end{pmatrix} \tag{13}$$

In the given expression, i = 0,1,2,3,…represent the nine discrete velocity directions in the D2Q9 model; c denotes the lattice speed, expressed as $c = \Delta x/\Delta t$. The weight coefficients w_i are assigned as follows: $w_0 = 4/9$, $w_{1\text{-}4} = 1/9$, $w_{5\text{-}8} = 1/36$; The lattice sound speed c_s is $1/\sqrt{3}$. The macroscopic velocity u and density ρ can be obtained through the following relationships.

$$\rho = \sum_i f_i \tag{14}$$

$$\rho u = \sum_i f_i e_i \tag{15}$$

Using the aforementioned relationships, through the Chapman-Enskog expansion[23,24], Eqs. (10) and (11) can be recovered into the mass and momentum conservation equations.

$$\partial_t \rho + \nabla \cdot (\rho \mathbf{u}) = 0 \tag{16}$$

$$\partial_t (\rho \mathbf{u}) + \nabla \cdot (\rho \mathbf{u}\mathbf{u}) = -\nabla p + \nabla \cdot \boldsymbol{\sigma} \tag{17}$$

In these equations, p denotes the fluid pressure and σ represents the viscous stress tensor.

Description of the LBM model for competitive gas adsorption

When gas adsorbates are transported to the surfaces of adsorbent particles through convection–diffusion, they are adsorbed at the contact points with the solid particle surface. The interaction between the gas adsorbates and the adsorbent particles constitutes a dynamic and reversible physical adsorption process, wherein adsorption and desorption behaviors coexist between the bulk gas phase and the pore walls. Therefore, by employing the derivation results under the monolayer assumption, the adsorption rate equation that characterizes the adsorption process on the adsorbent surface is presented as follows.

$$S_{C,A} = \partial N_A/\partial t = k_{a,A} C_A \left(V_m - V_A\right) - k_{d,A} V_A \left(1 + \frac{k_{a,B}}{k_{d,B}} C_B\right) \tag{18-1}$$

$$S_{C,B} = \partial N_B/\partial t = k_{a,B} C_B \left(V_m - V_B\right) - k_{d,B} V_B \left(1 + \frac{k_{a,A}}{k_{d,A}} C_A\right) \tag{18-2}$$

The adsorbates further diffuse from the outer surface of the adsorbent particles into the micropores within the adsorbent. Neglecting the impact of the internal micropore structure of the adsorbent particles, the diffusion process of adsorbates within the pores can be described using the Homogeneous Solid Diffusion Model (HSDM)[25]. The mass transport equation for this process is shown as:

$$\frac{\partial V}{\partial t} = D_p \left(\frac{\partial^2 V}{\partial x^2} + \frac{\partial^2 V}{\partial y^2}\right) \tag{19}$$

where D_p is the solid diffusion coefficient within the adsorbent particles.

In mass transfer physics problems, the D2Q5 lattice model is employed, utilizing direction vectors 0 through 4. This model effectively captures the essential dynamics of mass transfer processes within the defined lattice structure[26]. The evolution equations for the concentration of adsorbates in the bulk gas phase and the adsorbate content within the particles are approximated using the LBGK equation:

$$h_{i,n}\left(\mathbf{r} + e_i \Delta t, t + \Delta t\right) = h_{i,n}\left(r, t\right) - \frac{1}{\tau_{h,n}}\left[h_{i,n}\left(r, t\right) - h_{i,n}^{eq}\left(r, t\right)\right] + \omega_i S_{C,n} \Delta t \tag{20}$$

$$n_i\left(r + e_i \Delta t, t + \Delta t\right) = n_i\left(r, t\right) - \frac{1}{\tau_n}\left[n_i\left(r, t\right) - n_i^{eq}\left(r, t\right)\right] \tag{21}$$

In these equations, h_i and n_i are the distribution functions for the component concentration in the bulk gas phase and the adsorbate content within the particles, respectively. τ_h and τ_n are the corresponding dimensionless relaxation (collision) times. The equilibrium distribution functions, denoted as $h_i^{eq}(r,t)$ and $n_i^{eq}(r,t)$, are expressed as follows:

$$h_i^{eq}\left(r, t\right) = w_i C \left[1 + \frac{e_i \cdot u}{c_s^2}\right] \tag{21}$$

$$n_i^{eq}\left(r, t\right) = w_i N \tag{22}$$

where w_i are the weight coefficients, and in the D2Q5 model, $w_0 = 1/3$ and $w_{1\text{-}4} = 1/6$. Using the Chapman-Enskog expansion, the collision and evolution equations for the component concentration field and the adsorbate content can be recovered into the corresponding macroscopic equations through the following formulae:

$$D_s = c_s^2(\tau_h - 0.5)\Delta t,\ C = \sum_i h_i \tag{23}$$

$$D_p = c_s^2(\tau_n - 0.5)\Delta t,\ N = \sum_i n_i \tag{24}$$

Implementation of boundary conditions

Boundary treatment plays a crucial role in simulating flow and surface mass transfer in porous media. For flow problems, non-equilibrium extrapolation methods[27] are used for the inlet and outlet of the channel domain, with solid boundaries for the upper and lower boundaries and half step bounce-back boundary conditions. For mass transfer problems, detailed implementation of the concentration distribution function near the boundary requires careful analysis. Figure 2 illustrates concentration distribution functions on a fluid–solid boundary node under the D2Q5 model. The concentration distribution function on internal nodes of the fluid needs to be derived from the migration process of adjacent fluid nodes. But for fluid nodes near the boundary of particulate matter, the unknown concentration distribution function h_2 needs to be obtained through the following Eq. [28]

$$h_2 = h_4 - D_s \frac{\partial C_w}{\partial y} \tag{24}$$

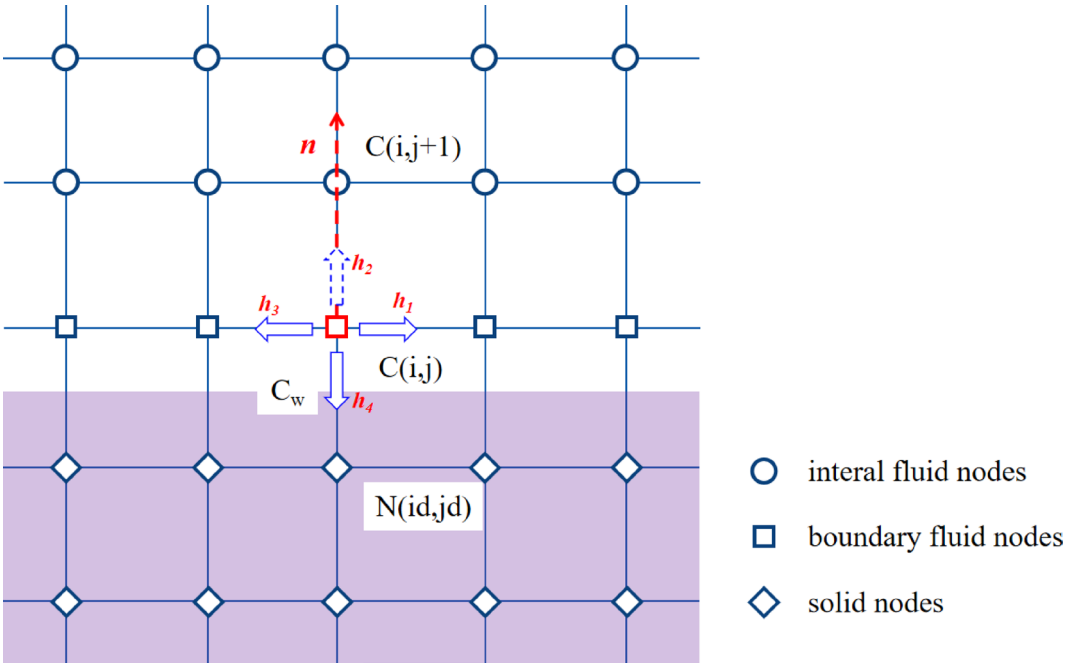

Fig. 2. Illustration of concentration distribution functions on a fluid–solid boundary.

Taking component A as an example, the Langmuir adsorption kinetics equation can be obtained from formulas (9–1) and (18–1)

$$D_s \frac{\partial C_A}{\partial n} = \frac{\partial N_A}{\partial t} = k_{a,A} C_A \left(N_m - N_A\right) - k_{d,A} N_A \left(1 + \frac{k_{a,B}}{k_{d,B}} C_B\right) \tag{25}$$

Finally, by using the finite difference scheme to match the concentration gradient along the normal direction of the wall, and substituting it into formula (24), the unknown distribution function h_2 on the boundary can be obtained.

Verification of the adsorption model

To verify the accuracy of the adsorption model under the simultaneous presence of convection, diffusion, and adsorption–desorption phenomena, we use the classical single-channel steady-state convection–diffusion system Lévêsque example to validate the LBM model algorithm[29]. The physical model is shown in Fig. 3.

The model dimensions are 320 × 320. Since steady-state pipe flow conforms to the characteristics of Poiseuille flow, a fully developed parabolic velocity profile is specified throughout the domain.

$$u\left(y\right) = -4u_{max} y\left(y - L\right)/L^2 \tag{26}$$

Maximum velocities are set at 0.02, 0.04, and 0.06, with a constant inlet concentration boundary condition C_0 set to 1. The concentration gradient is zero at the upper surface and outlet boundary, while adsorption occurs at the lower surface, which can be described using Henry's adsorption kinetic boundary condition:

$$D_s \frac{\partial C}{\partial y} = kC \tag{27}$$

where k is the Henry adsorption constant, set to 1.0 in this study; the adsorbate diffusion coefficient D_s is set to 1/6. The Lévêsque analytical solution for the steady-state Nondimensional mass at the lower surface is expressed as

$$\widetilde{C}_x = \frac{L}{C_0} \frac{\partial C}{\partial n} = 0.854 \left(\frac{u_{max} L^2}{x D_s}\right)^{1/3} \tag{28}$$

After the adsorption process reaches a steady state, the concentration field contour distribution of the LBM simulation results is shown in Fig. 4.

The comparison between the LBM simulation results and the Lévêsque analytical solution and simulation results of Zhou, etc.[30] shows that, apart from a slight discrepancy near the inlet at x = 0 due to singularities,

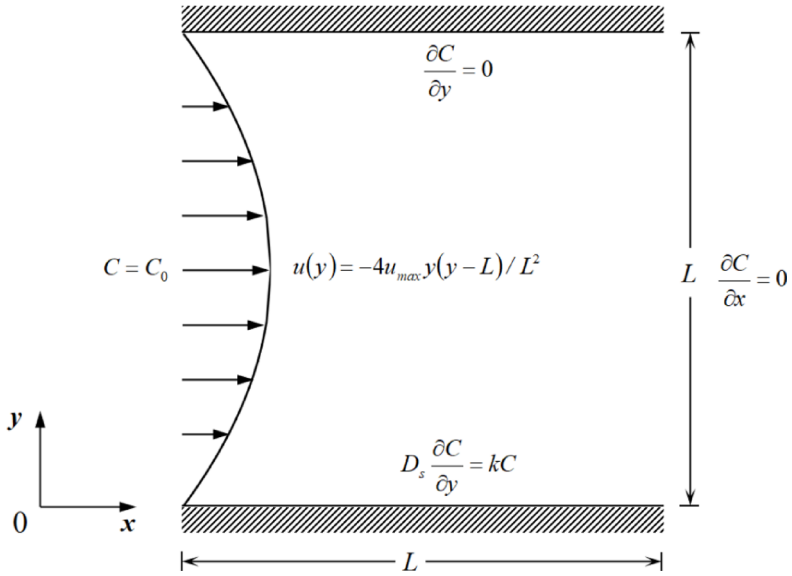

Fig. 3. Physical model of the Single-Channel Steady-State Convection–Diffusion system considering wall adsorption.

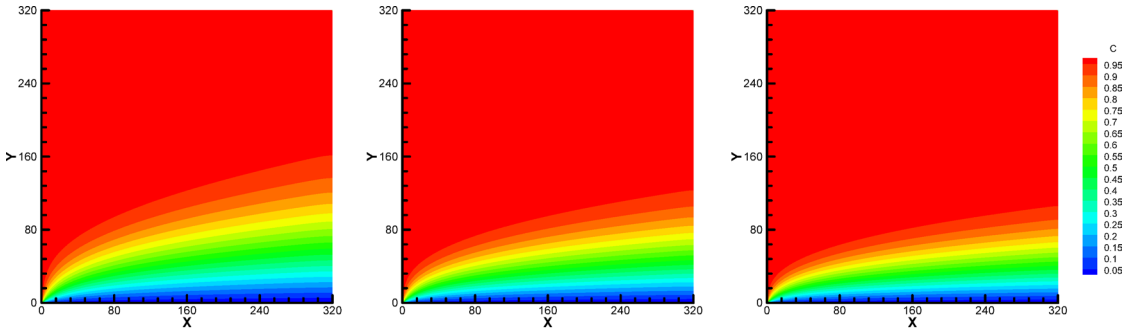

(a) u_{max}=0.02 (b) u_{max}=0.04 (c) u_{max}=0.06

Fig. 4. Contour plot of the concentration field in the Single-Channel Steady-State Convection–Diffusion process considering wall adsorption.

the results of both solutions are in close agreement (Fig. 5). This verifies the accuracy of the LBM method in simulating the coexistence of flow, diffusion, and interfacial adsorption effects.

Program validation and analysis of simulation results

Shale reservoir pressure usually ranges from 5 to 30 MPa and reservoir temperature mainly varies between 20 and 100 ℃[31]. In this study, a numerical simulation study was conducted on the CO_2 and CH_4 replacement processes, considering that the reservoir temperature is 50 ℃ and the reservoir pressure is 10 MPa (where the partial pressures of CO_2 and CH_4 are 5 MPa respectively).

The boundary conditions of the model are set in Table 1.

The physical model is built within a square channel of 100 × 100 lattice units. At the initial moment, the particles are adsorbed by the saturated CH_4 and CO_2 with a certain velocity and concentration is injected from the inlet on the left side of the flow field. The conversion between physical values and lattice values of simulation parameters is detailed in Table 2. Among them, the physical value of sound speed and kinematic viscosity are the average values of the two gases.

Adsorption/desorption characteristics of CO_2 displacing CH_4 in a single particle model

Considering shale particles with a diameter of 160nm (16 lattice units) in the flow field, the CO_2 injection concentration is 0.56kmol/m^3. Utilizing a binary gas competitive adsorption model, which incorporates adsorption and desorption behaviors (Eqs. 9–1 and 9–2), the LBM method is used to simulate these behaviors within the region of interest numerically.

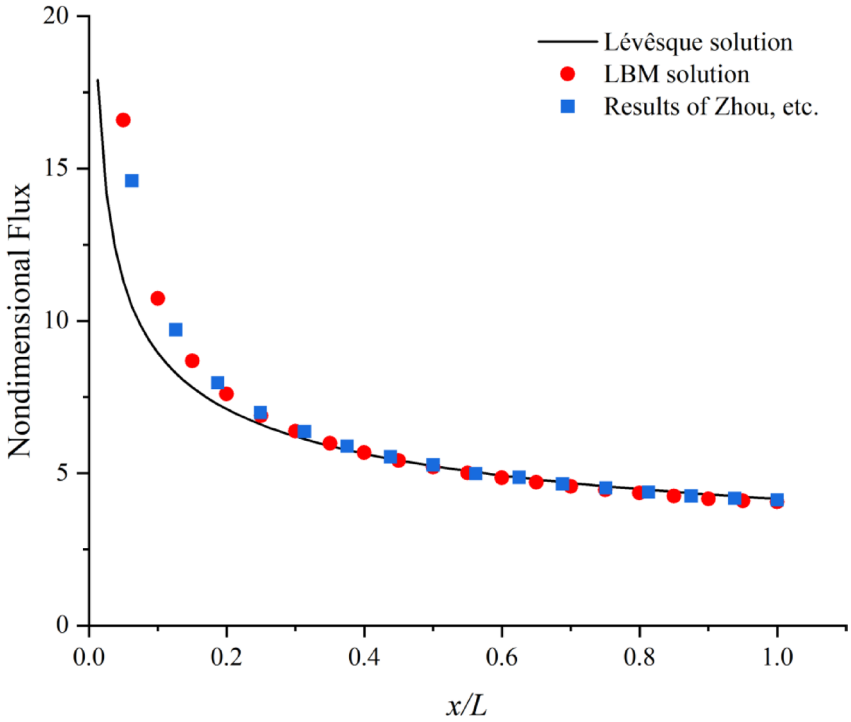

Fig. 5. Comparison of LBM simulated nondimensional mass flux as $u_{max} = 0.06$ with Lévêsque analytical solution and simulation results of Zhou, etc.

Boundary position	Boundary conditions
Inlet (left)	$u = u_0, C_1 = C_0, C_2 = 0$
Outlet (right)	$\partial u/\partial x = 0, \partial C_1/\partial x = 0, C_2/\partial x = 0$
Top wall	$u = 0, \partial C_1/\partial y = 0, \partial C_2/\partial y = 0$
Bottom wall	$u = 0, \partial C_1/\partial y = 0, \partial C_2/\partial y = 0$
Solid surfaces	$D_{s,1}\frac{\partial C_1}{\partial n} = k_{a,1}C_1(N_m - N_1) - k_{d,1}N_1\left(1 + \frac{k_{a,2}}{k_{d,2}}C_2\right), D_{s,2}\frac{\partial C_2}{\partial n} = k_{a,2}C_2(N_m - N_2) - k_{d,2}N_2\left(1 + \frac{k_{a,1}}{k_{d,1}}C_1\right)$

Table 1. Boundary conditions for simulation.

Figure 6 is the concentration distribution in the flow field and content in the particle of CH_4 and CO_2 at 1.123μs. The simulation results show that after CO_2 is injected from the left inlet, a higher CH_4 concentration appears in the flow field near the windward side of the adsorbent particles. This is because the adsorbent particles first come into contact with CO_2 on the windward side surface, and CO_2 begins to adsorb to the surface of the particles, while prompting rapid desorption of CH_4 inside the particles. It also shows that the injection of CO_2 significantly enhances the desorption ability of CH_4. CH_4 desorbed from particulate matter continuously diffuses into the surrounding flow field and migrates downstream through convection.

Due to the continuous desorption of methane on the surface of the particles, the methane content inside the particles continues to decrease, which causes the desorption power of CH_4 on the surface of the particles to continue to weaken, and the desorption speed also decreases. Eventually, CH_4 is completely desorbed from the particles, and the CH_4 concentration inside the particles and in the flow field gradually decreases to zero (as shown in Fig. 7).

As shown in Fig. 8, from the comparison curves of the content changes of CO_2 and CH_4 adsorbates in particulate matter and the adsorption/desorption rates, it can be seen that the process of CO_2 replacing CH_4 includes two different stages: the competitive adsorption stage and adsorption/desorption equilibrium stage. After CO_2 is injected, the adsorption process of CO_2 and the desorption process of CH_4 occur simultaneously. In the initial stage of competitive adsorption, the adsorption rate of CO_2 and the desorption rate of CH_4 both increase sharply, and the desorption rate value of CH_4 is slightly higher than the adsorption rate value of CO_2. It is worth noting that at about 0.558 μs, the curves of the CO_2 adsorption rate and the CH_4 desorption rate reach their extreme values at the same time. After that, the two values began to decrease and gradually decreased to zero, indicating that the two gases reached adsorption/desorption equilibrium. In this process, the desorption process of CH_4 reaches equilibrium before the adsorption process of CO_2.

Parameters	Symbol	Physical value	Unit	Lattice value	Scaling relation
Sound velocity	c_s	353	m/s	0.5774	–
Length	L	1.00E−06	m	100	$L = \Delta x\ L_l$
Width	H	1.00E−06	m	100	$H = \Delta y\ H_l$
Grid spacing	$\Delta x(\Delta y)$	1.00E−08	m	1	–
Time step	Δt	2.83E−11	s	1	$\Delta t = (\Delta x/c_s)\ \Delta t_l$
Kinematic viscosity	μ	2.82E−07	m^2/s	0.08	$\mu = (\Delta x^2/\Delta t)\ \mu_l$
CO_2 inlet velocity	v_0	0.2–0.6	m/s	0.0006–0.0018	$v = (\Delta x/\Delta t)\ v_l$
CH_4 saturated concentration	C_1	0.14	$kmol/m^3$	1	—
CO_2 saturated concentration	C_2	0.56	$kmol/m^3$	4	$C_2 = C_1\ C_{2l}$
CO_2 diffusion coefficient	$D1$	2.21E-07	m^2/s	0.063	$D = (\Delta x^2/\Delta t)\ D_l$
CH_4 diffusion coefficient	$D2$	5.11E-07	m^2/s	0.145	
CO_2 mass diffusion coefficient	D_{s1}	5.00E-09	m^2/s	0.0014	$D_s = (\Delta x^2/\Delta t)\ D_{sl}$
CH_4 mass diffusion coefficient	D_{s2}	3.00E-08	m^2/s	0.0085	
CO_2 adsorption rate constant	k_{a1}	2.21E + 09	m^3 /(kmol·s)	0.0088	$k_a = k_{al}\ /\ (C_1\ \Delta t)$
CH_4 adsorption rate constant	k_{a2}	2.21E + 09	m^3 /(kmol·s)	0.0088	
CO_2 desorption rate constant	k_{d1}	1.66E + 07	1/s	0.00047	$k_d = k_{dl}\ /\ \Delta t$
CH_4 desorption rate constant	k_{d2}	1.66E + 07	1/s	0.00047	
CH_4 Maximum adsorption	N_{max1}	0.14	$kmol/m^3$	1.0	$N_{max} = C_2 N_{maxl}$
CO_2 Maximum adsorption	N_{max2}	0.28	$kmol/m^3$	2.0	
Reynolds number	Re	0.75	—	0.75	—

Table 2. Conversion between physical values and lattice values of simulation parameters. Symbols with subscripts *l* are the lattice parameters. The relevant parameters are calculated from references[32–34] and NIST Physical Property Standards Database[35].

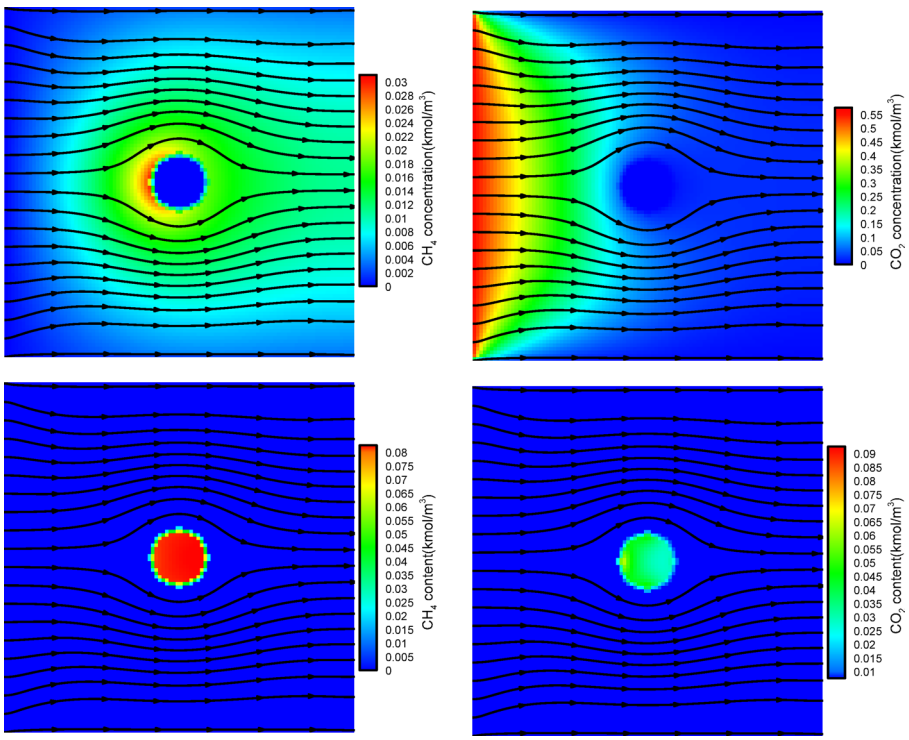

Fig. 6. Distribution of CH_4 and CO_2 concentration in flow field and CH_4 and CO_2 content in the particle at 1.123μs.

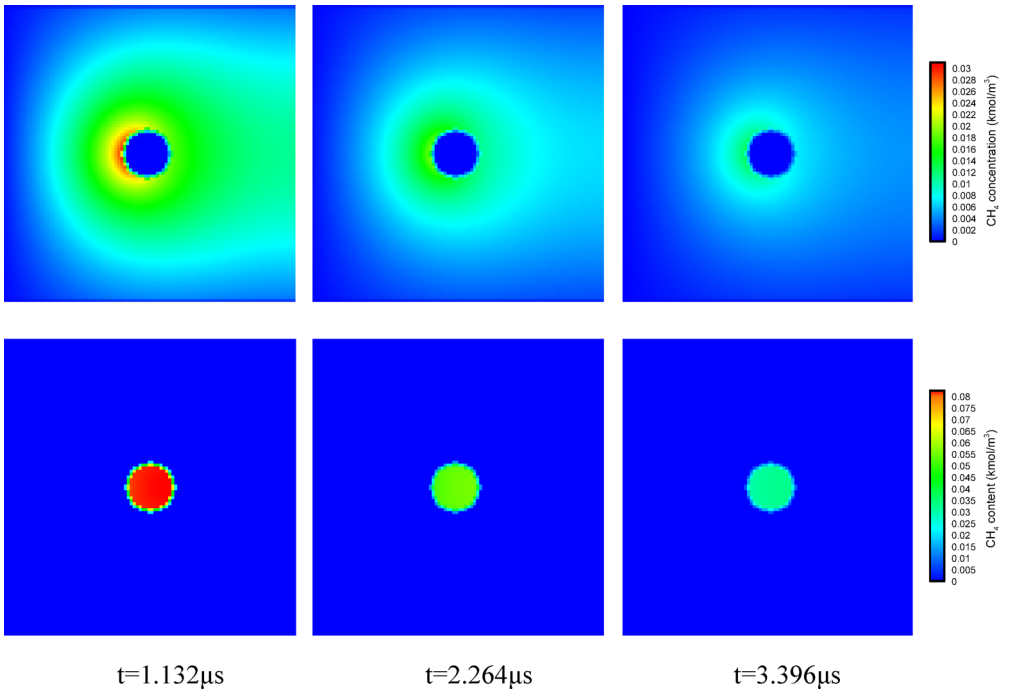

Fig. 7. Distribution of CH_4 concentration in flow field and CH_4 content in the particle at different time.

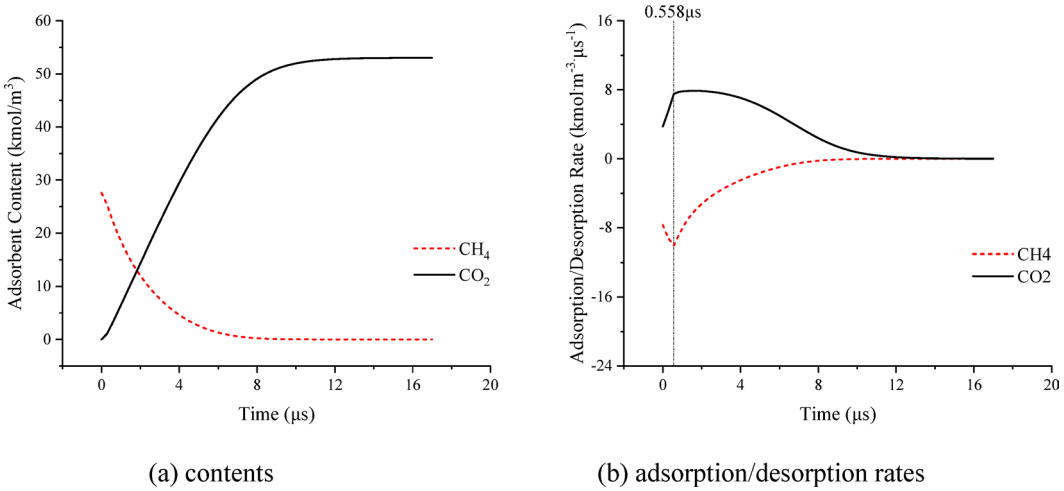

Fig. 8. Comparison of CO_2 and CH_4 contents and adsorption/desorption rates in particles over time.

In order to analyze the impact of the CO_2 concentration in the injected fluid on the CO_2 and CH_4 content in the particles, when the CO_2 concentration is 0kmol/m^3 (no carbon dioxide injection), 0.2kmol/m^3, 0.4kmol/m^3, and 0.6kmol/m^3, the model area Numerical simulations were performed. The study found that (as shown in Fig. 9), when there is no carbon dioxide injection, the CH_4 content in the particles decreases the slowest with time, indicating that the desorption rate of CH_4 is the slowest. The greater the CO_2 concentration of the injected fluid, the faster the CH_4 content in the particles decreases, indicating that the CH_4 desorption rate is faster and the time required to reach desorption equilibrium is shorter. Under corresponding conditions, the greater the CO_2 concentration of the injected fluid, the higher the CO_2 content in the particles. This indicates that the CO_2 adsorption rate is faster and the time required to reach desorption equilibrium is shorter.

Therefore, this model can effectively simulate the CO_2/CH_4 competitive adsorption phenomenon. Numerical results show that increasing the CO_2 concentration of the injected fluid can significantly promote the desorption of CH_4 and help improve the displacement efficiency of CO_2 to CH_4.

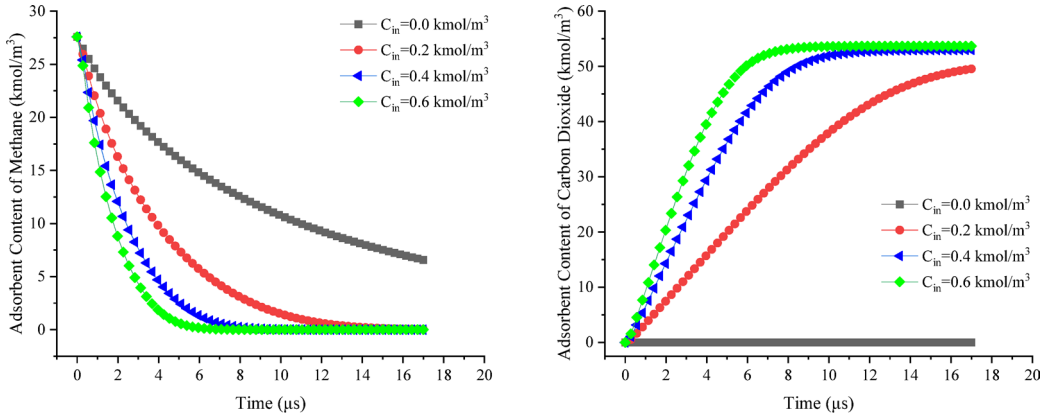

(a) content of CH_4 (b) content of CO_2

Fig. 9. Comparison of changes in the content of CH_4 and CO_2 adsorbates inside the particles as different CO_2 injection concentration.

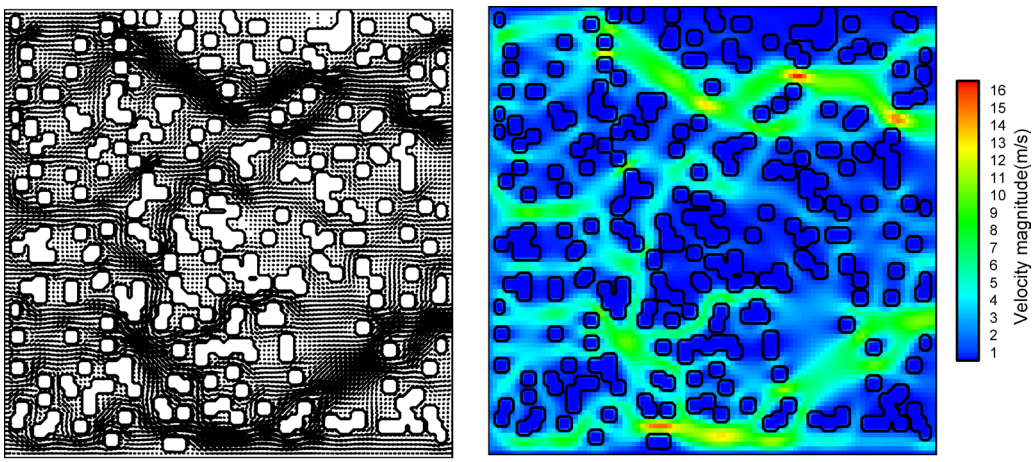

(a) velocity vector distribution (b) velocity magnitudes distribution

Fig. 10. Distribution of vectors and magnitudes of fluid velocity.

Adsorption/desorption characteristics of CO_2 displacing CH_4 in a porous media model

The process of CO_2 displacing CH_4 is a key feature of CO_2-ESGR technology. Combined with the binary gas adsorption rate equation, the LBM method was used to numerically simulate the physical process of CO_2 displacing CH_4 accompanied by adsorption and desorption behavior in the porous media model. The physical model is established within a square channel of 100 nm × 100 nm. The initial adsorbed CH_4 content in the particles is set at 0.14kmol/m^3, and CO_2 with a concentration of 0.4kmol/m^3 is injected at the Re number about 0.25–0.75. Due to the pore structure's inhomogeneity, significant velocity changes are observed throughout the flow field. Areas characterized by low permeability exhibit lower fluxes and flow rates, while areas with high permeability exhibit higher fluxes and flow rates, as shown in Fig. 10.

From a time evolution perspective, the migration and distribution of CO_2 concentration are significantly affected by the flow velocity. In the high flow rate area, the fluid flux increases and the CO_2 concentration migrates faster. On the contrary, in the low flow rate area, the fluid flux increases and the CO_2 concentration migrates faster. In addition, CO_2 in the flow field also migrates through self-diffusion. Therefore, the concentration gradient near the front of the CO_2 concentration distribution is large, significantly higher than the concentration gradient at the rear (as shown in Fig. 11).

The spatial and temporal evolution of CH_4 and CO_2 concentrations (as shown in Fig. 12) shows that the concentrations of the two gases are complementary. Regions with high CO_2 concentration have low CH_4 concentration and vice versa. As time goes on, CO_2 gradually occupies the pore space, displacing CH_4.

The behavior of CO_2 displacing CH_4 within the pores is more pronounced in the concentration changes within the particles. As shown in Fig. 13, over time, the CO_2 content within the particles increases while the CH_4 content decreases. This complementary distribution further demonstrates that CO_2 injection facilitates CH_4 desorption.

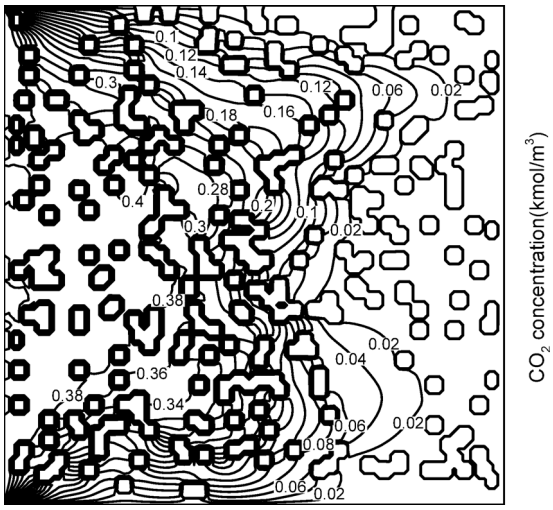

Fig. 11. Contour line of CO_2 concentration in the flow field at 22.66μs.

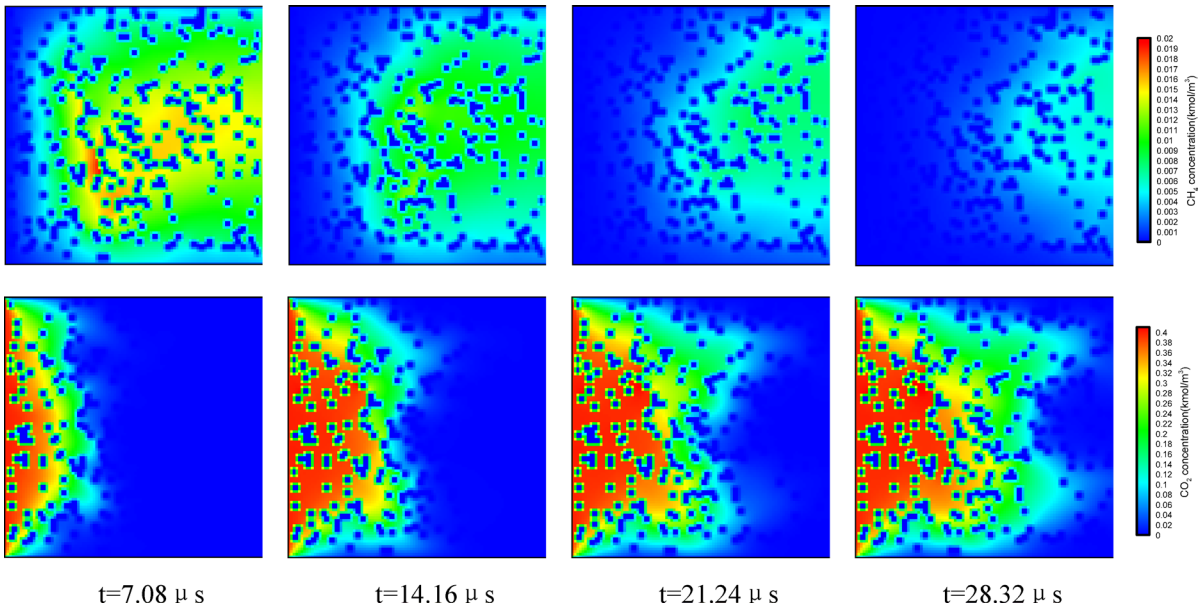

Fig. 12. Distribution of CH_4 and CO_2 concentration in flow field at different time.

Three porosity models (0.64, 0.76, and 0.89) were employed to numerically simulate the CO_2 displacing CH_4 process to investigate further porosity's impact on the adsorption and desorption characteristics of porous media. By comparing the CO_2 concentration distribution in the flow field with the spatiotemporal distribution of CO_2 content within the porous media matrix (as shown in Fig. 14), it was observed that the CO_2 concentration distribution in the flow field significantly influences the distribution of adsorbate CO_2 content within the pore matrix. The evolution of these distributions occurs almost synchronously in both space and time.

Related studies have shown that in high porosity materials, the surface diffusion rate of CO_2 may be increased due to enhanced pore connectivity[36], while in low porosity media, gas diffusion is limited by narrow pore throat structures, resulting in slow adsorption desorption rates[37]. From the simulation results in this article, it can be seen that models with higher porosity exhibit better permeability, while the diffusion rate of adsorbates is faster and the displacement efficiency is higher, which is consistent with the conclusions in the literature and further confirms the correctness of the theoretical model derived in this article.

Furthermore, increased porosity correlates with a reduced time required to achieve adsorption/desorption equilibrium for CO_2 and CH_4. Under identical CO_2 injection concentrations, models with higher porosity more readily attain adsorption/desorption equilibrium, and the total adsorption amount at equilibrium is lower (as illustrated in Fig. 15).

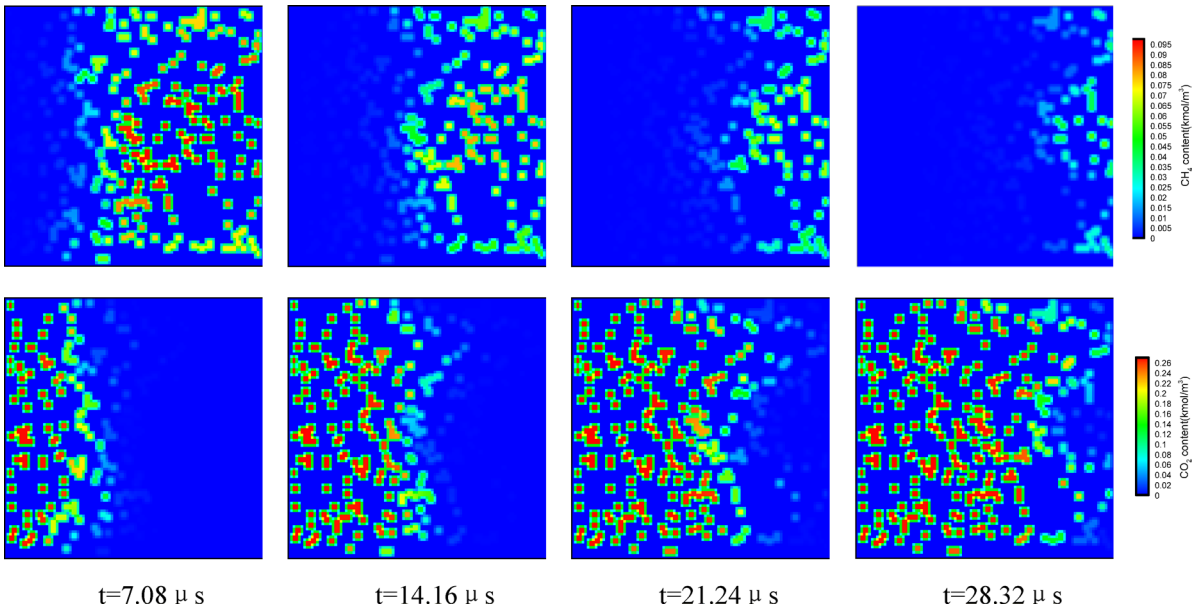

Fig. 13. Distribution of CH_4 and CO_2 content in particles at different time.

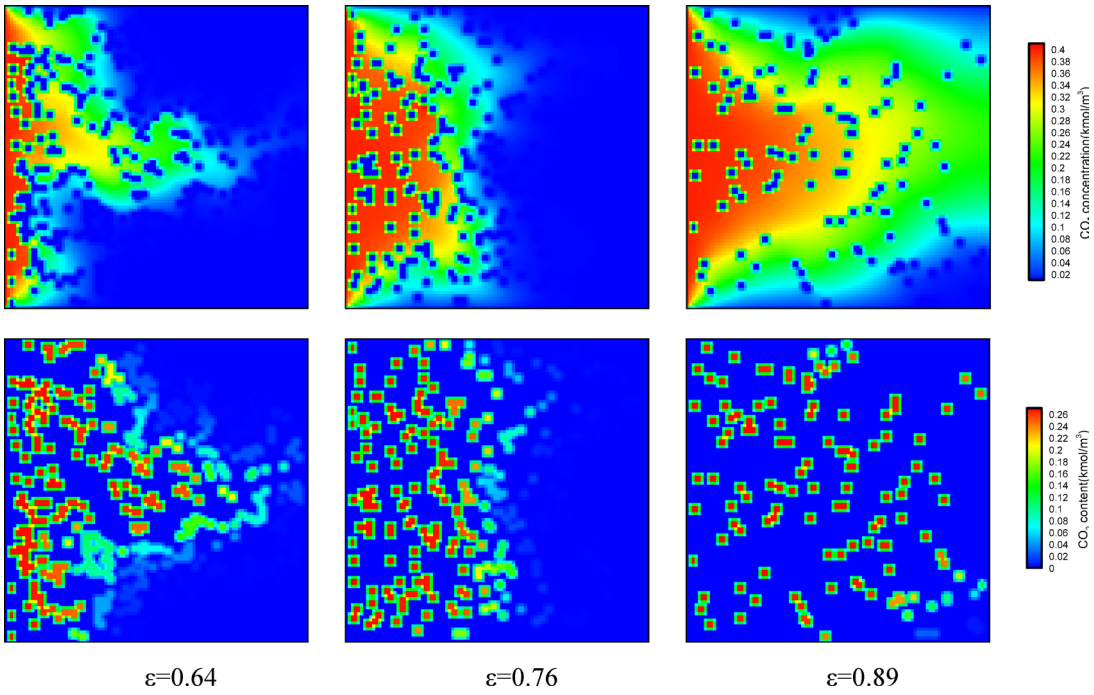

Fig. 14. Distribution of CO_2 concentration in flow field and CO_2 content inside particles at 14.16μs for different porosity.

Conclusion

In this study, the lattice-Boltzmann method (LBM) was utilized to simulate the flow, diffusion, and related adsorption/desorption behaviors during the displacement process of CO_2/CH_4 gases in a porous adsorption system at the pore scale. The primary research findings and conclusions are as follows:

(1) The theoretical formula of the binary gas competitive adsorption rate model was derived, and this formula was applied to the lattice Boltzmann method (LBM) to simulate the displacement process of CH_4 by CO_2. The research results show that the obtained theoretical model can truly reflect the competitive adsorption behavior between CO_2 and CH_4, and helps analyze the adsorption and desorption characteristics in the process of CO_2 displacing CH_4.

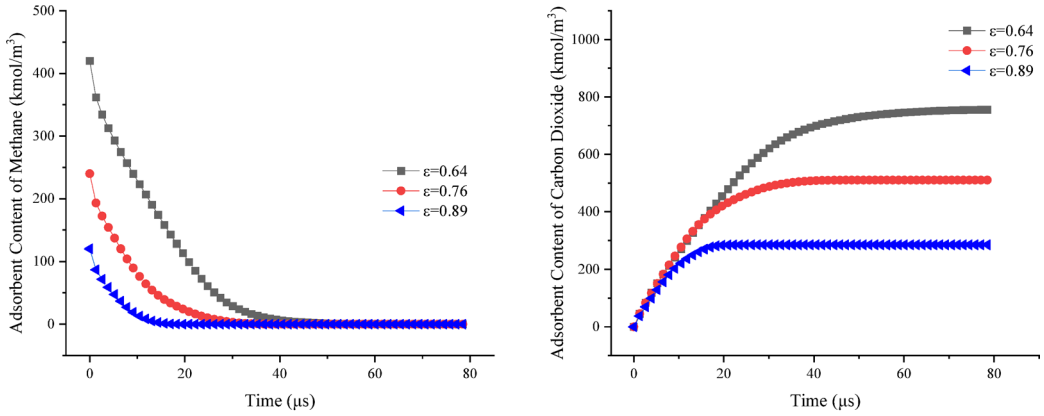

(a) content of CH_4 (b) content of CO_2

Fig. 15. Changes in CH_4 and CO_2 content inside particles with different porosity over time.

(2) The process of CO_2 displacing CH_4 is a dynamic process in which CO_2 adsorption and CH_4 desorption occur simultaneously. The injected CO_2 is gradually adsorbed by the particles, occupying the original CH_4 adsorption sites. CH_4 inside the particles is gradually desorbed and migrates downstream through convection and diffusion in the flow field. It is worth noting that both gases eventually reach the adsorption/desorption equilibrium state, and CO_2 reaches adsorption equilibrium slightly later than CH_4 reaches desorption equilibrium.

(3) The injection concentration of CO_2 will significantly affect the characteristics of the CO_2/CH_4 displacement process. The higher the concentration of injected CO_2, the shorter the time required for CO_2/CH_4 to reach adsorption and desorption equilibrium, indicating that increasing the CO2 injection concentration can increase the CO_2 adsorption rate and CH_4 desorption rate, thus promoting the adsorption of CO_2 and the desorption of CH_4. Therefore, the replacement efficiency of CH_4 by CO_2 can be effectively improved by increasing the concentration of carbon dioxide in the injection.

(4) Models with higher porosity exhibit better permeability, resulting in faster diffusion rates of adsorbate and increased displacement efficiency. The heterogeneity of pore structure significantly affects the velocity distribution in the flow field, and then plays a dominant role in the distribution of CO_2 and CH_4 concentration fields. The concentrations of CH_4 and CO_2 in the flow field and the contents of CO_2 and CH_4 in the particles show obvious complementarity and synchrony in the spatial and temporal distribution. This observation further demonstrates that CO_2 injection can promote CH_4 desorption, thereby helping to improve shale gas recovery.

Data availability

The datasets used and/or analysed during the current study available from the corresponding author on reasonable request.

Received: 6 March 2025; Accepted: 1 January 2026
Published online: 12 January 2026

References

1. Zhao, Y. et al. Competitive adsorption of CH_4/CO_2 in shale nanopores during static and displacement process. *Natural Gas Indus. B* **11**, 239–251 (2024).
2. Li, J. et al. N_2 influences on CH_4 accumulation and displacement in shale by molecular dynamics. *Sci. Rep.* **15**, 1833 (2025).
3. Biagi, J., Agarwal, R. & Zhang, Z. Simulation and optimization of enhanced gas recovery utilizing CO2. *Energy* **94**, 78–86 (2016).
4. Sun, H., Yao, J. & Yalchin, E. Upscaling of gas transport in shale matrix based on homogenization theory. *Sci. Sin.-Phys. Mech. Astron.* **47**, 114612 (2017).
5. Wu, J., Gan, Y., Shi, Z., Huang, P. & Shen, L. Pore-scale lattice Boltzmann simulation of CO_2-CH_4 displacement in shale matrix. *Energy* **278**, 127991 (2023).
6. Li, N. et al. Micro-mechanical properties of shale due to water/supercritical carbon dioxide-rock interaction. *Pet. Explor. Dev.* **50**, 1001–1012 (2023).
7. Tian, S., Jia, H., Ge, Z., Wang, G. & Bai, R. Experimental study on the CH_4/CO_2 competitive adsorption behaviors of typical shale minerals in low pressure reservoirs. *Fuel* **390**, 134765 (2025).
8. Wang, Z., Sang, S., Zhou, X. & Liu, X. Numerical study on CO_2 sequestration in low-permeability coal reservoirs to enhance CH4 recovery: Gas driving water and staged inhibition on CH4 output. *J. Petrol. Sci. Eng.* **214**, 110478 (2022).
9. He, Y., Li, Q., Wang, Y. & Tang, G. Lattice Boltzmann method and its applications in engineering thermophysics. *Chin. Sci. Bull.* **54**, 4117–4134 (2009).
10. Ren, L., Fu, Y., Hu, Y. & Zhao, J. Simulation of Microscopic Gas Flowing in Shale Based on LBM. *Spec. Oil Gas Reserv.* **24**, 70–75 (2017).
11. Luo, Z., Luo, Q., Xu, H. & Yang, M. LBM Simulation of Heat and Mass Double Diffusion, Fluid-Solid Conjugate Heat Transfer and Adsorption. *Chin. J. Comput. Phys.* **36**, 60–68 (2019).

12. Yang, H. et al. Lattice Boltzmann simulation of CO_2 adsorption by ZIF-8 porous materials. *J. Chin. Soc. Power Eng.* **43**, 1363–1370 (2023).
13. Cai, P., Que, Y., Jiang, Z. & Yang, P. Lattice Boltzmann meso-seepage research of reconstructed soil based on the quartet structure generation set. *Hydrogeol. Eng. Geol.* **49**, 33–42 (2022).
14. Zhou, L., Qu, Z. G., Ding, T. & Miao, J. Y. Lattice Boltzmann simulation of the gas-solid adsorption process in reconstructed random porous media. *Phys. Rev. E* **93**, 043101 (2016).
15. Wang, J., Duan, Z., Yuan, Y. & Xue, H. Lattice Boltzmann simulation of dynamic adsorption and desorp- tion characteristics of LNG boil-off gas at low temperature. *J. Eng. Thermal Energy Power* **38**, 137–146 (2023).
16. Xu, C. et al. Feasibility of the CO_2-ESGR technique for providing carbon-negative shale gas: A life cycle assessment. *J. Clean. Prod.* **484**, 144353 (2024).
17. Hajianzadeh, M., Mahmoudi, J. & Sadeghzadeh, S. Molecular dynamics simulations of methane adsorption and displacement from graphenylene shale reservoir nanochannels. *Sci. Rep.* **13**, 15765 (2023).
18. Zakirov, T. R. & Khramchenkov, M. G. Effect of pore space heterogeneity on the adsorption dynamics in porous media at various convection-diffusion and reaction conditions: A lattice Boltzmann study. *J. Petrol. Sci. Eng.* **212**, 110300 (2022).
19. Do, D. D. & Wang, K. A new model for the description of adsorption kinetics in heterogeneous activated carbon. *Carbon* **36**, 1539–1554 (1998).
20. Langmuir, I. The adsorption of gases on plane surfaces of glass, mica and platinum. *J. Am. Chem. Soc.* **40**, 1361–1403 (1918).
21. Hu, B. W. & Wang, J. G. Fractal microstructure effects on effective gas diffusivity of a nanoporous medium based on pore-scale numerical simulations with lattice Boltzmann method. *Phys. Rev.* **104**, 065304 (2021).
22. Qian, Y. H., D'Humières, D. & Lallemand, P. Lattice BGK Models for Navier-Stokes Equation. *Europhys. Lett.* **17**, 479–484 (1992).
23. Chapman, S., Cowling, T. G. & Park, D. The Mathematical Theory of Non-Uniform Gases. *Am. J. Phys.* **30**, 389–389 (1962).
24. Frisch, U. Relation between the lattice Boltzmann equation and the Navier-stokes equations. *Physica D* **47**, 231–232 (1991).
25. Chahbani, M. H., Labidi, J. & Paris, J. Effect of mass transfer kinetics on the performance of adsorptive heat pump systems. *Appl. Therm. Eng.* **22**, 23–40 (2002).
26. Liu, P. Y., Ju, L., Pu, J. & Guo, Z. L. Numerical study on the effects of fracture on density-driven flows in CO2 sequestration. *Phys. Fluids* **36**, 046615 (2024).
27. Guo, Z. L., Zheng, C. G. & Shi, B. C. An extrapolation method for boundary conditions in lattice Boltzmann method. *Phys. Fluids* **14**, 2007–2010 (2002).
28. Kang, Q. J., Lichtner, P. C. & Zhang, D. X. An improved lattice Boltzmann model for multicomponent reactive transport in porous media at the pore scale. *Water Resour. Res.* **43**, 2578–2584 (2007).
29. Machado, R. Numerical simulations of surface reaction in porous media with lattice Boltzmann. *Chem. Eng. Sci.* **69**, 628–643 (2012).
30. Zhou, L. et al. Lattice Boltzmann simulation of gas-solid adsorption processes at pore scale level. *J. Comput. Phys.* **300**, 800–813 (2015).
31. Jiang, S. et al. Occurrence of normally-pressured shale gas in China and the United States and their effects on mobility and production: A case study of southeast Sichuan Basin and Appalachia Basin. *Petrol. Reserv. Eval. Dev.* **12**, 399–406 (2022).
32. Higashi, H. & Tamura, K. Calculation of diffusion coefficient for supercritical carbon dioxide and carbon dioxide+naphthalene system by molecular dynamics simulation using EPM2 model. *Mol. Simul.* **36**, 772–777 (2010).
33. Scheiner, B. & Yoon, T. J. Calculation of self-diffusion coefficients in supercritical carbon dioxide using mean force kinetic theory. *J. Chem. Phys.* **154**, 134101 (2021).
34. Huber, M. L., Lemmon, E. W., Bell, I. H. & McLinden, M. O. The NIST REFPROP Database for Highly Accurate Properties of Industrially Important Fluids. *Ind. Eng. Chem. Res.* **61**, 15449–15472 (2022).
35. Lemmon, E., Huber, M. & Mclinden, M. NIST reference fluid thermodynamic and transport properties-REFPROP. *NIST Standard Reference Database*.
36. Song, W. H., Yao, J. & Zhang, K. Study on gas adsorption and transport behavior in shale organic nanopore. *Chin. J. Theor. Appl. Mech.* **53**, 2179–2192 (2021).
37. Kong, D. L. et al. Deposition of titanium oxide films by atmospheric pressure corona discharge plasma jet. *Acta Physica Sinica* **70**, 095205 (2021).

Acknowledgements

This work was supported by the Natural Science Foundation of Hunan Province (Grant: 2021JJ30206 and 2025JJ60312); National Natural Science Foundation of China (Grant: 52504281); Scientific Research Foundation of Hunan Provincial Education Department (Grant: 21A0572); Changsha Municipal Natural Science Foundation (Grant: kq2502022); College Students Innovation and Entrepreneurship Training Program of Hunan Province (Grant: S202311528144 and S202511528170).

Author contributions

Yifu Zhang, Yu Xu and Xuefeng Chen wrote the main manuscript text and Zikun Pi, Qiannan Xie and Kunpeng Liao prepared Figs. 1, 2, 3, 4, 5, 6, 7, 8, 9, 10, 11, 12, 13 and 14. All authors reviewed the manuscript.

Declarations

Competing interests

The authors declare that they have no known competing financial interests or personal relationships that could have appeared to effect the work reported in this paper.

Additional information

Correspondence and requests for materials should be addressed to Y.X.

Reprints and permissions information is available at www.nature.com/reprints.

Publisher's note Springer Nature remains neutral with regard to jurisdictional claims in published maps and institutional affiliations.